p14–MP1-MEK1 signaling regulates endosomal traffic and cellular proliferation during tissue homeostasis

David Teis,[1] Nicole Taub,[1] Robert Kurzbauer,[5] Diana Hilber,[1] Mariana E. de Araujo,[1] Miriam Erlacher,[2] Martin Offterdinger,[1] Andreas Villunger,[2] Stephan Geley,[3] Georg Bohn,[6] Christoph Klein,[6] Michael W. Hess,[4] and Lukas A. Huber[1]

[1]Division of Cell Biology, [2]Division of Experimental Pathophysiology and Immunology, and [3]Division of Molecular Pathophysiology, Biocenter, and [4]Department of Anatomy, Histology, and Embryology, Innsbruck Medical University, A-6020 Innsbruck, Austria
[5]Institute of Molecular Pathology, 1-1030 Vienna, Austria
[6]Department of Pediatric Hematology and Oncology, Hannover Medical School, D-30625 Hannover, Germany

The extracellular signal-regulated kinase (ERK) cascade regulates proliferation, differentiation, and survival in multicellular organisms. Scaffold proteins regulate intracellular signaling by providing critical spatial and temporal specificity. The scaffold protein MEK1 (mitogen-activated protein kinase and ERK kinase 1) partner (MP1) is localized to late endosomes by the adaptor protein p14. Using conditional gene disruption of *p14* in mice, we now demonstrate that the p14–MP1-MEK1 signaling complex regulates late endosomal traffic and cellular proliferation. This function its essential for early embryogenesis and during tissue homeostasis, as revealed by epidermis-specific deletion of *p14*. These findings show that endosomal p14–MP1-MEK1 signaling has a specific and essential function in vivo and, therefore, indicate that regulation of late endosomal traffic by extracellular signals is required to maintain tissue homeostasis.

Introduction

The extracellular signal-regulated kinase (ERK) cascade consists of the kinases Ras-activated factor (RAF), MEK (MAPK and ERK kinase), and ERK. They are coupled to a great variety of upstream activators and downstream effectors that regulate proliferation, differentiation, and survival in multicellular organisms. Mammalian cells contain three members of the RAF family (Raf-1, B-Raf, and A-Raf), two different MEK proteins (MEK1 and MEK2), and two ERK proteins (ERK1 and ERK2). These kinase isoforms appear very similar with regard to their structural and biochemical properties and, thus, do not reveal how the ERK cascade acquires signaling specificity to execute context-specific physiological functions (Kolch, 2000).

Signaling specificity could be mediated by scaffold and adaptor proteins that trigger the formation of specific signaling complexes at different subcellular locations (Morrison and Davis, 2003; Teis and Huber, 2003). Two scaffold proteins are known to facilitate ERK activation in mammalian cells: the kinase suppressor of Ras 1 (KSR1) and MEK1 partner (MP1). KSR1 was identified as a positive modulator of Ras/MAPK signaling (Kornfeld et al., 1995; Therrien et al., 1995). Upon EGF stimulation, KSR1 is recruited to the plasma membrane, where it enhances MEK and ERK activation (Muller et al., 2001). MP1 was identified in a yeast two-hybrid screen as a specific binding partner of MEK1 (Schaeffer et al., 1998). MP1 is recruited to late endosomes by the adaptor protein p14 (Teis et al., 2002). MP1 and p14 are structurally almost identical and form a very stable heterodimeric complex (Kurzbauer et al., 2004) that is required for ERK activation on endosomes (Teis et al., 2002; Pullikuth et al., 2005). However, the biological significance of p14–MP1-facilitated ERK signaling was not known, and it was unclear whether KSR and the p14–MP1 complex would function in a redundant manner.

In this study, we show that the p14–MP1-MEK1 complex is specifically required to regulate endosomal traffic and cellular proliferation. Conditional gene targeting of *p14* in mice reveals its essential function during early embryogenesis and skin

D. Teis and N. Taub contributed equally to this paper.

Correspondence to Lukas A. Huber: Lukas.A.Huber@i-med.ac.at

Abbreviations used in this paper: EGFR, EGF receptor; ERK, extracellular signal-regulated kinase; KSR, kinase suppressor of Ras; LBPA, lysobisphosphatidic acid; MEF, mouse embryonic fibroblast; MEK, MAPK and ERK kinase; MORE, Mox2Cre; MP1, MEK1 partner; MVB, multivesicular body; RAF, Ras-activated factor; wt, wild type.

The online version of this article contains supplemental material.

The Journal of Cell Biology, Vol. 175, No. 6, December 18, 2006 861–868
http://www.jcb.org/cgi/doi/10.1083/jcb.200607025

Table I. **Offspring analysis of $p14^{-/-}$ mice**

Age of crosses	$p14^{+/+}$	$p14^{-/+}$	$p14^{-/-}$	$p14^{f/-}$	$p14^{f/+}$
$p14^{-/+} \times p14^{-/+}$					
E6.5 ($n = 29$)	6	15	8	ND	ND
E8.5 ($n = 50$)	13	25	12	ND	ND
E10.5 ($n = 70$)	19	51	0	ND	ND
PN21 ($n = 210$)	70	140	0	ND	ND
$p14^{-/f} \times p14^{-/+}$;MORE					
E10.5 ($n = 30$)	ND	13	0	7	10
PN21 ($n = 56$)	0	20	0	17	19

$p14^{-/+}$ intercrosses were analyzed at different developmental stages. Before E6.5, no phenotypic abnormalities of the embryos could be detected. Upon E10.5, no $p14^{-/-}$ embryos could be detected. The epiblast-restricted deletion of p14 caused the embryonic lethality of $p14^{-/-}$ mice resulting from $p14^{-/f} \times p14^{-/+}$;MORE crosses. The numbers of embryos at the indicated developmental stages are given. PN, postnatal.

development. These findings demonstrate a crucial function of the p14–MP1-MEK1 signaling complex in the regulation of tissue homeostasis.

Results and discussion

p14 is required for early embryonic development

We investigated the biological function of the endosomal adaptor protein p14 by generating mice that carry a floxed *p14* allele. The single mouse *p14* gene (geneID 83409) is located on chromosome 3 and is ubiquitously expressed (Wunderlich et al., 2001). Exons 1–4 of *p14* were flanked by *lox*P sites to create a conditional allele (Fig. S1, A–C; available at http://www.jcb.org/cgi/content/full/jcb.200607025/DC1).

To determine whether p14 was essential for mouse development, heterozygous $p14^{-/+}$ mice were intercrossed. No homozygous $p14^{-/-}$ mice were identified in a total of >200 offspring (Table I). Instead, $p14^{-/+}$ mice were born at a 2:1 ratio over their wild-type (wt) littermates, which was a clear indication of embryonic lethality. Embryos from $p14^{-/+}$ intercrosses were analyzed at different embryonic stages. No phenotypic abnormalities could be detected at embryonic day (E) 6.5. At E8.5, ~25% of the embryos ($n = 50$) were grossly growth retarded with severe developmental defects and were homozygous mutants (Fig. 1 A). By E10.5, no $p14^{-/-}$ embryos were detected ($n = 70$; Table I). To assess whether the death of $p14^{-/-}$ embryos was caused by placental defects, we used Mox2Cre (MORE) mice to delete *p14* specifically in the epiblast (Tallquist and Soriano, 2000). Epiblast-restricted p14 deletion also caused embryonic lethality before E10.5 ($n = 86$; Table I). These data suggested that the embryonic lethality of $p14^{-/-}$ mice was not caused by placental defects but was the result of defects in the developing embryo.

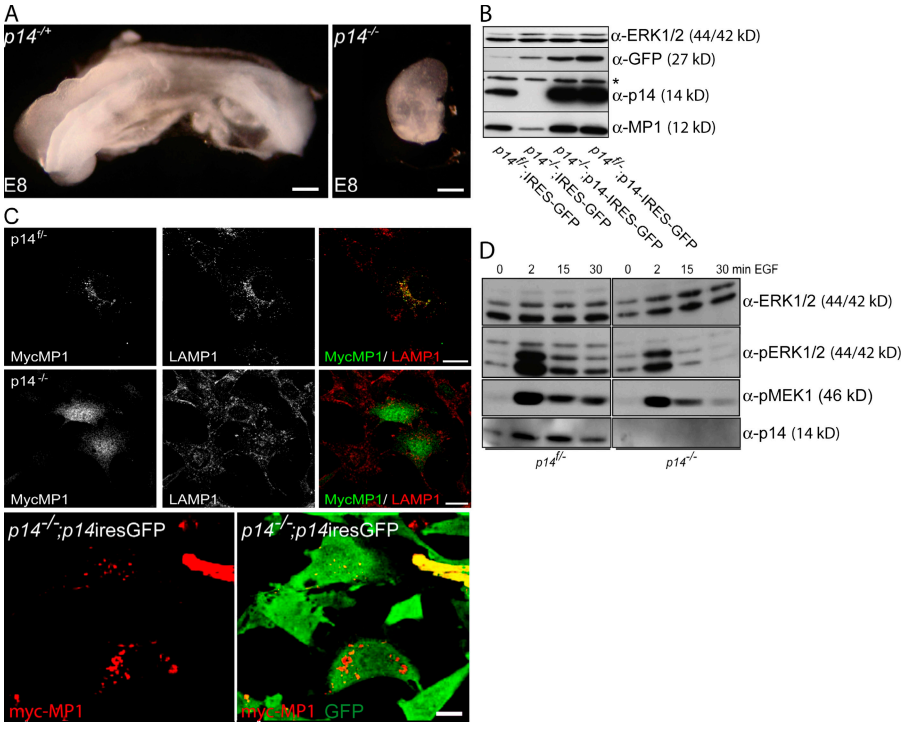

Figure 1. ***p14* is an essential gene required for embryonic development and endosomal ERK activation.** (A) Homozygous $p14^{-/-}$ embryos die around gastrulation. Representative $p14^{-/-}$ and $p14^{-/+}$ E8 embryos are shown. (B) $p14^{f/-}$ and $p14^{-/-}$ MEFs were infected with either control retrovirus (IRES-GFP) or p14 retrovirus (p14-IRES-GFP). $p14^{f/-}$;IRES-GFP, $p14^{-/-}$;IRES-GFP, $p14^{-/-}$;p14-IRES-GFP, and $p14^{f/-}$;p14-IRES-GFP cell lysates were separated by SDS-PAGE, analyzed by Western blotting, and probed with the indicated antibodies. The asterisk marks the background band of the p14 antibody. (C) $p14^{f/-}$ and $p14^{-/-}$ MEFs were infected with myc-MP1 retrovirus. myc-MP1 (green) colocalizes with LAMP1 (red) in $p14^{f/-}$ (top) and mislocalizes to the cytoplasm in $p14^{-/-}$ MEFs (middle). $p14^{-/-}$ MEFs were infected with p14-IRES-GFP retrovirus (green), transfected with myc-MP1 (red), and analyzed by immunofluorescence microscopy using anti-myc antibodies. (bottom) (D) $p14^{f/-}$ and $p14^{-/-}$ MEFs were starved overnight and stimulated with 100 ng/ml EGF for the indicated times. Cell lysates were separated by SDS-PAGE, analyzed by Western blotting, and probed with the indicated antibodies. Bars (A), 300 μm; (C), 10 μm.

The p14–MP1-MEK1 signaling complex regulates late endosomal traffic

Next, we generated immortalized $p14^{-/-}$ mouse embryonic fibroblasts (MEFs) to determine the cellular function of p14. E1A-immortalized $p14^{f/-}$ MEFs were infected with an adenovirus-expressing Cre. These MEFs ($p14^{-/-}$ MEFs) were devoid of p14 protein (Fig. 1 B) and mRNA (not depicted). Interestingly, the protein levels of the p14 interaction partner MP1 were also considerably reduced in the absence of p14, whereas protein levels of ERK1/2 were not affected (Fig. 1 B).

Ectopically expressed myc-MP1 localized to late endosomes in $p14^{f/-}$ MEFs, whereas myc-MP1 mislocalized to the cytoplasm in $p14^{-/-}$ MEFs (Fig. 1 C). Reexpression of p14 restored MP1 protein levels (Fig. 1 B, third lane) and its endosomal localization (Fig. 1 C). Thus, p14 is essential to recruit MP1 to late endosomes, which, in turn, is required for efficient and sustained EGF-induced MEK and ERK signaling (Fig. 1 D).

The p14–MP1 heterodimer interacts with MEK1 (Schaeffer et al., 1998; Teis et al., 2002; Pullikuth et al., 2005). Because MEK1 has been implicated in regulating endosomal dynamics and Golgi disassembly during mitosis (Acharya et al., 1998; Pelkmans et al., 2005), we next asked whether the p14–MP1-MEK1 complex regulates endosomal transport.

The steady-state localization of early endosomes (EEA1) was not altered in $p14^{-/-}$ and $Mek1^{-/-}$ MEFs (Fig. 2 A). However, late endosomes, multivesicular bodies (MVBs; lysobisphosphatidic acid [LBPA]), and lysosomes (LAMP1) were displaced to the cell periphery (Fig. 2 A, arrows). Reexpression of p14 restored the perinuclear localization of late endosomes (Fig. 2 C). A mutant p14caax, which resides at the plasma membrane (Teis et al., 2002), did not restore proper endosomal

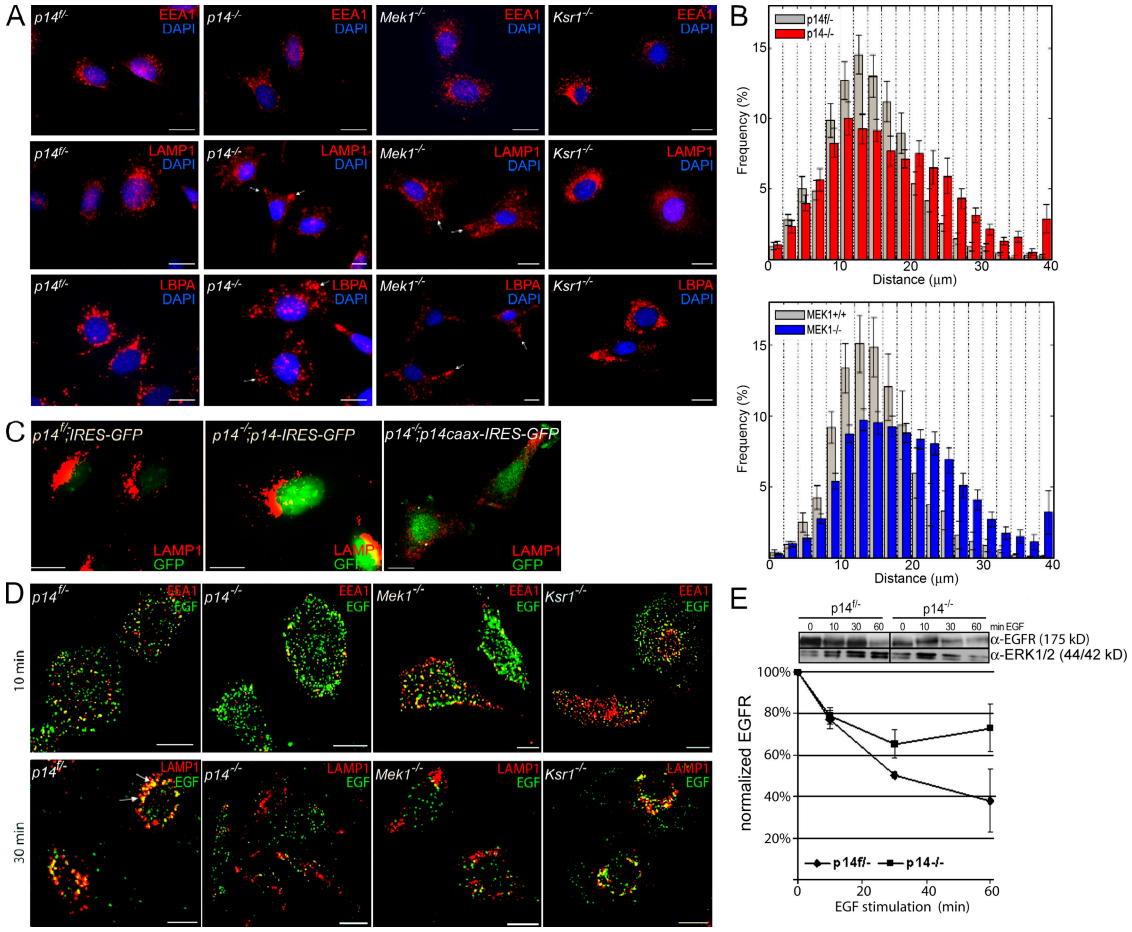

Figure 2. **p14 is required for late endosomal positioning and EGFR transport.** (A) $p14^{f/-}$ and $p14^{-/-}$ as well as $MEK1^{-/-}$ and $KSR1^{-/-}$ MEFs were subjected to immunofluorescence analysis with the indicated antibodies. EEA1, LAMP1, and LBPA are shown in red, and nuclei are stained with DAPI (blue). (B) Distribution analysis of LAMP1-positive endosomes in $p14^{f/-}$ and $p14^{-/-}$ $MEK1^{+/+}$ and $MEK1^{-/-}$ MEFs. The distance distribution of LAMP1-positive endosomes to the nucleus is shown. (C) $p14^{f/-}$ were infected with control retrovirus (IRES-GFP), and $p14^{-/-}$ MEFs were infected with retrovirus-expressing p14 (p14;IRES-GFP) or p14caax (p14caax;IRES-GFP) and subjected to immunofluorescence analysis. LAMP1 is shown in red, and GFP expression from different IRES-GFP retroviruses indicates p14 or p14caax expression. (D) $p14^{f/-}$, $p14^{-/-}$, $MEK1^{-/-}$, and $KSR1^{-/-}$ MEFs were starved overnight and stimulated with 100 ng/ml of fluorescently labeled EGF. Cells were fixed at the indicated times and subjected to confocal immunofluorescence analysis with the indicated antibodies. EGF is shown in green, and EEA1 and LAMP1 are shown in red. Colocalization of EGF with either EEA1 or LAMP1 is shown in yellow (arrows). (E) $p14^{f/-}$ and $p14^{-/-}$ MEFs were starved overnight and stimulated with 100 ng/ml EGF for the indicated times. Cell lysates were separated by SDS-PAGE, analyzed by Western blotting, and probed with the indicated antibodies. One representative EGFR immunoblot is shown. The EGFR degradation was analyzed in three independent experiments, and EGFR protein levels were normalized to total ERK protein levels. The graph shows the mean EGFR degradation in $p14^{f/-}$ and $p14^{-/-}$ MEFs. Error bars represent SD. Bars, 10 μm.

localization (Fig. 2 C). This finding demonstrates a crucial role of p14 in the regulation of late endosomes. To investigate whether the positioning of late endosomes requires p14–MP1-MEK1 signaling, we determined the localization of MVBs and lysosomes in MEFs in which *MEK1* was deleted (*Mek1*$^{-/-}$ MEFs; Fig. 2 A). MVBs and lysosomes were displaced to the cell periphery in *Mek1*$^{-/-}$ MEFs (Fig. 2 A, arrows), which is reminiscent of their mislocalization in *p14*$^{-/-}$ MEFs. Early as well as late endosomes and lysosomes were not affected in *KSR1*$^{-/-}$ MEFs (Fig. 2 A).

An endosome distribution analysis was performed to determine the position of late endosomes and lysosomes (LAMP1) relative to the nucleus (Fig. 2 B and Fig. S2 B, available at http://www.jcb.org/cgi/content/full/jcb.200607025/DC1). In *p14*$^{f/-}$ and *Mek1*$^{+/+}$ MEFs, ~80% of late endosomes and lysosomes were located in a perinuclear region (within 20 μm of the nucleus), and 20% were >20 μm away. Notably, ~40% of all late endosomes and lysosomes in the *p14*$^{-/-}$ and *Mek1*$^{-/-}$ MEFs were >20 μm away from the nucleus. However, the total number of late endosomes and lysosomes was not changed (Fig. 2 B and Fig. S2 B). These findings indicate that the p14–MP1-MEK1 complex but not KSR1 is required to regulate the distribution of late endosomes.

To determine whether the p14–MP1-MEK1 signaling complex is required for efficient transport from early endosomes to late endosomes and lysosomes, we used different endocytic cargos. The p14–MP1-MEK1 complex does not regulate the uptake or endosomal traffic of transferrin or dextran (Fig. S2 A). EGF-induced endocytosis of the EGF receptor (EGFR) into early endosomes was not affected (Fig. 2 D, 10 min). In *p14*$^{f/-}$ and *KSR1*$^{-/-}$ MEFs, EGF colocalized with LAMP1-positive late endosomes (Fig. 2 D, 30 min; arrows). However, no colocalization of EGF with LAMP1 was detected in *p14*$^{-/-}$ and *Mek1*$^{-/-}$ MEFs (Fig. 2 D, 30 min). To further assess the defect in endocytic EGFR traffic, we used quantitative immunoblot analysis of EGFR degradation (Fig. 2 E and Fig. S2 C). 60 min after EGF stimulation, >60% of total EGFR was degraded in the *p14*$^{f/-}$ MEF, whereas only 30% of total EGFR was degraded in the *p14*$^{-/-}$ MEF (Fig. 2 E and Fig. S2 B). Together, these findings show that late endosomal sorting of activated cell surface receptors is a specific function of the p14–MP1-MEK1 signaling complex.

p14 is required for epidermal development

We next addressed how altered late endocytic traffic and reduced ERK signaling would affect tissue homeostasis. Because EGFR and ERK signaling are critical regulators of epidermal proliferation and differentiation, we performed the conditional deletion of *p14* in the epidermis. *p14*$^{f/f}$ were crossed with K5-Cre2 transgenic mice (Tarutani et al., 1997) and bred further to generate *p14*$^{f/f}$;K5-Cre2 (*p14*$^{\Delta ep}$) animals. PCR analysis from epidermal DNA and Western blot analysis from epidermal lysates demonstrated that *p14* was specifically deleted in the epidermis but not in the dermis (Fig. 3 F and Fig. S1, D and E). *p14*$^{\Delta ep}$ mice were born alive but died shortly after birth. E18.5 embryos were alive but displayed dramatic skin defects. *p14*$^{\Delta ep}$ skin appeared erythemic and moist as compared with *p14*$^{\Delta ep/+}$ control littermates (Fig. 3 A). The *p14*$^{\Delta ep}$ epidermis consisted of only a few (four or less) cell layers, and nucleated cells were frequently found in the uppermost cell layer (Fig. 3 A, arrow).

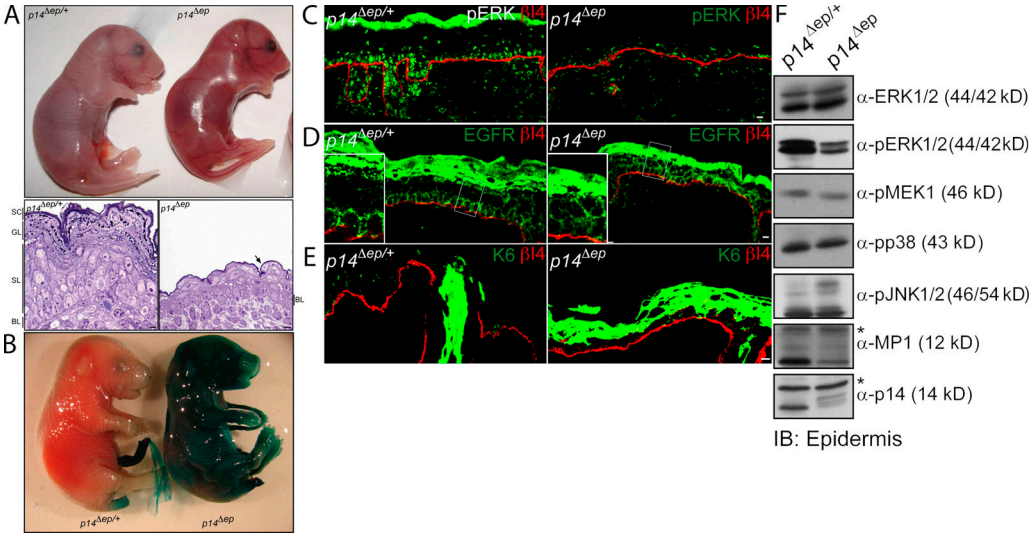

Figure 3. **The p14–MP1 complex is required for epidermal development and regulates ERK signaling and EGFR degradation.** (A) Representative phenotype of E18.5 *p14*$^{\Delta ep/+}$ and *p14*$^{\Delta ep}$ embryos. Semithin sections of E18.5 *p14*$^{\Delta ep}$ and *p14*$^{\Delta ep/+}$ skin were stained with Toluidine blue. The *p14*$^{\Delta ep/+}$ skin consists of stratum corneum (SC), granular layers (GL), spinous layers (SL), and the basal layer (BL). *p14*$^{\Delta ep}$ lacks the stratum corneum and granular layer. The arrow indicates a nucleated cell in the uppermost layer of *p14*$^{\Delta ep}$ skin. (B) E18.5 *p14*$^{\Delta ep}$ and *p14*$^{\Delta ep/+}$ embryos were subjected to an epidermal barrier assay. X-Gal fully penetrated the *p14*$^{\Delta ep}$ epidermis of embryos. (C–E) Frozen skin sections from E18.5 *p14*$^{\Delta ep}$ and *p14*$^{\Delta ep/+}$ embryos were analyzed by confocal laser-scanning immunofluorescence microscopy. β4-Integrin is shown in red. Bars, 10 μm. (C) pERK1/2 (green) is strongly reduced in the basal compartment of *p14*$^{\Delta ep}$ epidermis. Note the unspecific background staining in the stratum corneum in panel *p14*$^{\Delta ep/+}$. (D) EGFR (green) is present at the plasma membrane of suprabasal keratinocytes in the *p14*$^{\Delta ep}$ epidermis. Insets show magnifications of boxed areas. (E) Keratin 6 is shown in green and is normally confined to the innermost cell layer of the outer root sheath. (F) Equal protein amounts of epidermal lysates from E18.5 *p14*$^{\Delta ep}$ and *p14*$^{\Delta ep/+}$ embryos were analyzed by Western blotting with the indicated antibodies. Asterisks indicate the background bands of the p14 and MP1 antibodies.

The stratum corneum and granular layers were not defined. This indicated compromised terminal differentiation, which resulted in a fatal skin barrier defect (Fig. 3 B) and rapid dehydration, finally causing the perinatal death of the $p14^{\Delta ep}$ mice. These findings demonstrated an essential function of p14 in the development of the epidermis.

The p14–MP1-MEK1 complex is required for ERK signaling and regulates EGFR degradation during epidermal development

Immunofluorescence (Fig. 3 C) and Western blot analysis from epidermal lysates (Fig. 3 F) demonstrated that p14 is specifically required for MEK and ERK activation in the epidermis but does not affect the p38 or JNK pathway. Because p14–MP1-MEK1 signaling is required to regulate transport of the EGFR to late endosomes, we next asked whether the fatal failure of epidermal development is caused by aberrant EGFR traffic. Consistent with previously published results (Sibilia and Wagner, 1995), the EGFR was expressed in the basal cell layer of $p14^{\Delta ep/+}$ epidermis (Fig. 3 D, inset). However, in $p14^{\Delta ep}$ epidermis, EGFR expression was not restricted to the basal cell layer and extended frequently into suprabasal cell layers (Fig. 3 D, inset), indicating an impaired degradation of EGFR. The failure to down-regulate the EGFR in the suprabasal cell layers resulted in unscheduled and strong suprabasal keratin 6 expression (Fig. 3 E). Keratin 6 expression is known to be induced by suprabasal EGFR expression (Jiang et al., 1993). The expression of keratins 14, 10, and 1 was only mildly affected (Fig. S1 G). Thus, impairment of late endosomal transport and subsequent suprabasal accumulation of the EGFR might result in unscheduled keratin 6 expression, which caused the disastrous failure of the epidermal development of $p14^{\Delta ep}$ animals.

The p14–MP1 complex regulates cellular proliferation

Induction of keratin 6 indicates a pathological status of the epidermis and is frequently associated with hyperproliferation. However, the $p14^{\Delta ep}$ epidermis was much thinner compared with the $p14^{\Delta ep/+}$ epidermis (Fig. 3 A). Cell death was not increased as monitored by TUNEL analysis and activated caspase-3 immunofluorescence staining (Fig. S1 H). Therefore, we investigated whether cell cycle progression was affected in the $p14^{\Delta ep}$ epidermis.

To detect keratinocytes in S phase, pregnant animals at 18.5 d of gestation were injected with BrdU. 1 h later, embryonic skin was collected and analyzed by immunofluorescence analysis. BrdU-positive cells resided in the basal cell layer of $p14^{\Delta ep/+}$ and $p14^{\Delta ep}$ epidermis. The number of BrdU-positive cells in the $p14^{\Delta ep}$ epidermis was reduced to 54% (Fig. 4, A and C). The mitotic index of the epidermis was determined by immunofluorescence microscopy with antiphosphohistone H3 antibody. Mitotic cells localized to the basal layer of $p14^{\Delta ep/+}$ and $p14^{\Delta ep}$ epidermis. The number of mitotic cells in the $p14^{\Delta ep}$ epidermis was reduced to 50% (Fig. 4, B and C). These findings suggested that endosomal p14–MP1-MEK1 signaling regulates proliferation in the epidermis.

Next, we asked whether the regulation of proliferation was a general and cell-autonomous function. Isolated $p14^{\Delta ep}$

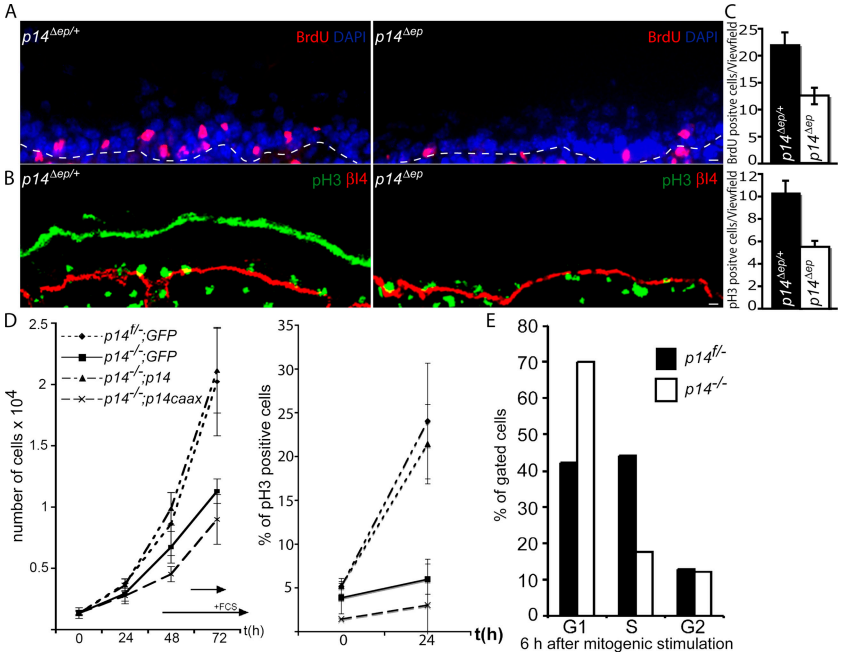

Figure 4. **The p14–MP1 complex regulates cell cycle progression and cellular proliferation.** (A and B) Frozen skin sections from E18.5 $p14^{\Delta ep}$ and $p14^{\Delta ep/+}$ embryos were analyzed by confocal immunofluorescence microscopy and quantification. Representative images are shown. Bars, 10 µm. (A) DAPI is shown in blue, and BrdU is shown in red. The dotted white line indicates the epidermal–dermal boundary. (B) β4-Integrin is shown in red, and phosphohistone H3 is shown in green. Note the unspecific background staining in the stratum corneum in panel $p14^{\Delta ep/+}$. (C) BrdU-positive cells were quantified in 25 random fields of view from four different embryos. In the $p14^{\Delta ep/+}$ epidermis, 22 ± 2.2 (SD [error bars]) cells/field of view were BrdU-positive cells. In the $p14^{\Delta ep}$ epidermis, 12 ± 1.51 (54.5%) were BrdU positive. Phosphohistone H3 (pH3)–positive cells were quantified in 58 random fields of view from six different embryos. The mean per field of view was 10 ± 1.1 phosphohistone H3–positive cells (100%) in the $p14^{\Delta ep/+}$ epidermis and 5 ± 0.57 (50%) in the $p14^{\Delta ep}$ epidermis. $P < 0.001$. (D) 0.5×10^4 $p14^{f/-}$;IRES-GFP, $p14^{-/-}$;IRES-GFP, $p14^{-/-}$;p14-IRES-GFP, and $p14^{-/-}$;p14caax-IRES-GFP MEFs were plated. Cells were counted at the indicated times. On day 4, $p14^{f/-}$;IRES-GFP had grown to 2.02×10^4 MEFs (100 ± 21%), $p14^{-/-}$;IRES-GFP had grown to 1.10^4 MEFs (54.4 ± 8%), $p14^{-/-}$;p14-IRES-GFPhad grown to 2.10^4 MEFs (103 ± 16%), and $p14^{-/-}$;p14caax-IRES-GFP had grown to 0.9×10^4 MEFs (44.5 ± 22%; $n = 3$). Growth-arrested MEFs were released into S phase. The number of mitotic cells was analyzed by DAPI and phosphohistone H3 staining. Mitotic indexes before the release (t = 0) were as follows: $p14^{f/-}$;IRES-GFP, 5.2 ± 0.2% ($n = 166$); $p14^{-/-}$;IRES-GFP, 3.8 ± 1.8% ($n = 300$); $p14^{-/-}$;p14-IRES-GFP, 5.2 ± 0.8% ($n = 325$); and $p14^{-/-}$;p14caax-IRES-GFP, 1.4 ± 0.2% ($n = 260$). 24 h after the release (t = 24 h), mitotic indexes were as follows: $p14^{f/-}$;IRES-GFP, 24 ± 4.5% ($n = 122$); $p14^{-/-}$;IRES-GFP, 6 ± 1.7% ($n = 83$); $p14^{-/-}$;p14-IRES-GFP, 21 ± 6.6% ($n = 109$); and $p14^{-/-}$;p14caax-IRES-GFP, 3% ($n = 42$). (E) Quantitative analysis by propidium iodide FACS of the DNA content of $p14^{f/-}$ and $p14^{-/-}$ MEFs 6 h after mitogenic stimulation. Results for $p14^{f/-}$ and $p14^{-/-}$ MEFs, respectively, were as follows: G1 phase, 42.2 and 70%; S phase, 44.2 and 17.7%; and G2–M phase, 12.8 and 12.2% ($n = 3$).

keratinocytes exhibited no or extremely poor growth. Therefore, we used MEFs to determine whether p14 regulates proliferation. An equal number of $p14^{f/-}$ and $p14^{-/-}$ MEFs were plated and grown for 3 d. After 3 d, $p14^{f/-}$ MEFs grew twice as fast compared with $p14^{-/-}$ MEFs (Fig. 4 D). Importantly, the growth defect in continuously growing cultures was fully restored by the retroviral reexpression of wt p14 in $p14^{-/-}$ MEFs (Fig. 4 D).

To address whether cellular proliferation requires the endosomal localization of p14, we used the p14caax mutant, which efficiently retargets the p14–MP1 complex from endosomes to the plasma membrane (Wunderlich et al., 2001). The p14caax mutant could not rescue the growth defect of $p14^{-/-}$ MEFs (Fig. 4 D). This indicates that only an endosomal p14–MP1 complex provides certain spatial information that is required for cell cycle progression. These findings substantiated a link between endosomal signaling and the regulation of proliferation.

To determine the mitotic index, MEFs were growth arrested by contact inhibition and 48-h serum starvation. MEFs were released from the growth arrest by subconfluent replating in either FCS- or EGF-containing medium (EGF data is not depicted; results were similar to those from FCS-treated cells). After 24 h in FCS, the mitotic $p14^{f/-}$ MEFs had increased from 5 to 24%, whereas the number of mitotic $p14^{-/-}$ MEFs changed from 4 to 6% (Fig. 4 D). Expression of the mutant p14caax did not restore the defects in mitotic entry (Fig. 4 D) nor did the overexpression of MEK1 or MP1 in $p14^{-/-}$ MEFs (not depicted). The reexpression of p14 in $p14^{-/-}$ MEFs fully restored mitogenic proliferation (Fig. 4 D), showing that endosomal p14–MP1-MEK1 signaling regulates proliferation in a cell-autonomous manner. The defects of mitogenic entry were also reflected by reduced BrdU incorporation after mitogenic stimulation (Fig. S1 F), indicating a delay in S-phase entry. Next, we determined how the loss of p14 would affect entry into mitosis upon mitogenic stimulation using propidium iodide FACS analysis. 6 h after release from the growth arrest into FCS-containing medium, 44% of the $p14^{f/-}$ MEFs had entered S phase. In contrast, only 17% of the $p14^{-/-}$ MEFs had entered S phase, and 70% were still in G1 phase (Fig. 4 E).

In conclusion, p14 is the adaptor protein that recruits the scaffold protein MP1 to late endosomes. There, MP1 interacts with MEK1, which, in turn, controls the late endosomal traffic of activated cell surface receptors and endosomal ERK activation. This provides the spatial and temporal resolution of ERK signaling that is required to promote proliferation in vivo. Thus, our findings indicate that cells coordinate extracellular signaling and endosomal traffic to regulate proliferation during tissue homeostasis.

Materials and methods

Targeting constructs

The HSV-Tk cassette for negative selection and an FRT-NEO-FRT *lox*P cassette were gifts from M. Busslinger (Institute of Molecular Pathology, Vienna, Austria). The IRES-hrGFP-SV40polyA cassette was from Vitality hrGFP (Stratagene). The genomic locus of p14 was amplified from HM-1 (E14.1 derivative) DNA with Herculase (Stratagene). All cassettes and the genomic locus for the targeting vector were cloned into pSP64 vector with a modified polylinker. The 5′ *lox*P site was inserted before exon 1. The IRES-driven hrGFP was inserted to follow p14 promoter activity upon deletion. The 5-kb-long arm was generated using three PCRs: primers (all sequences are listed in the supplemental material, available at http://www.jcb.org/cgi/content/full/jcb.200607025/DC1) 152–153, 154–181, and 180–193. The intermediate fragment, the four exons, and poly-A was amplified by PCR using primers 188–194 and was flanked 5′ by a *lox*P site. The short arm of the targeting vector was generated by PCR using the primers 184–185 and cloned 3′ of the FRT-NEO-FRT *lox*P and IRES-hrGFP cassette. Gene targeting was performed in HM-1 (E14.1 derivative) embryonic stem cells by electroporating the linearized targeting construct. For selection, 300 μg/ml G418 was used, and clones were screened by PCR and Southern blot analysis. Chimeric mice were created by the injection of two independent targeted embryonic stem cell clones into C57BL/6 blastocysts.

PCR genotyping, Southern blots, and Western blots

For genotyping, DNA was extracted from tails according to standard protocols. For genotyping of the epidermis tail, the epidermis was separated from dermis by dispase II (Roche) digest, and DNA was extracted according to standard protocols. For Southern blots, 10 μg KpnI-digested DNA were probed by using a 450-bp external probe (primers 219–220). Primer sequences are listed in the supplemental material. Western blots were performed as previously described (Teis et al., 2002).

Histology, semithin sections, and immunofluorescence

Isolated skin pieces were embedded in optimal cutting temperature–Tissue-Tek on dry ice. Immunofluorescence was performed on 6-μm frozen sections as previously described (Vasioukhin et al., 2001) and were analyzed using a confocal microscope (LSM510 Meta; Carl Zeiss MicroImaging, Inc.; for details, see supplemental material). For semithin section microscopy, skin was fixed with glutaraldehyde (2.5% vol/vol in 0.1 M sodium cacodylate buffer, pH 7.4) followed by unbuffered aqueous osmium tetroxide (1% wt/vol) and unbuffered aqueous uranyl acetate (0.5% wt/vol). Specimens were embedded in Epon epoxy resin. 500-nm semithin sections were stained with Toluidine blue. Immunofluorescence on MEFs was performed as previously described (Teis et al., 2002) and was analyzed using a microscope (Axioplan2 or confocal LSM510 Meta; Carl Zeiss MicroImaging, Inc.; for details, see supplemental material).

Antibodies and endocytic cargos

Primary antibodies were used according to the manufacturer's instructions. Anti-ERK1/2, antiphospho-ERK1/2, antiphospho-AKT, antiphospho-MEK1/2, antiphospho-p38, and antiphospho-JNK1/2 were purchased from Cell Signaling Technology. Antikeratins 1, 6, 10, and 14 were obtained from Covance. Anti–β-integrin 4 and anti–mouse Lamp1 antibody were purchased from BD Biosciences. Anti-Ki67 was obtained from Novacastra, anti-BrdU was purchased from Roche, and antiphosphohistone 3 was purchased from Upstate Biotechnology. Anti-EGFR and -EEA1 antibodies were obtained from Fitzgerald and Santa Cruz Biotechnology, Inc., and anti-LAMP1 was purchased from BD Biosciences. The LBPA antibody was a gift from J. Gruenberg (University of Geneva, Geneva, Switzerland). Anti-p14 and -MP1 antibodies were described previously (Teis et al., 2002). Fluorescently labeled secondary antibodies are listed in the supplemental materials. MEFs were stimulated with 50 ng/ml AlexaFluor594-transferrin or 100 ng/ml of fluorescently labeled EGF for 10 and 30 min or were incubated with 3 mg/ml AlexaFluor488-dextran for 15 and 45 min.

BrdU labeling

Pregnant animals at day 18.5 of gestation were injected intraperitoneally with 1 ml/100 g bodyweight of a 10-mM BrdU (Roche) solution. Embryonic skin was removed and embedded in optimal cutting temperature–Tissue-Tek. Tissue culture cells were incubated for 30 min with 10 μM BrdU. Samples were processed according to the manufacturer's instructions.

Isolation of epidermis

To separate the epidermis from dermis, skin was incubated (dermis facing down) in Dispase II (Roche) for 30 min at 32°C. To extract proteins, isolated epidermis was incubated in protein lysis buffer (50 mM Tris-HCl, 200 mM NaCl, 1% Triton X-100, 10% glycerol, 5 mM $Na_4P_2O_7$, 2 mM Na_3OV_4, 50 mM NaF, 20 mM β-glycerophosphate, and protease inhibitors) and mechanically disrupted using a mixer mill tissue homogenizer (MM 301; Retsch).

Generation of the p14 knockout cell line and MEF cell culture

MEFs were generated from day 13.5 $p14^{f/-}$ embryos. $p14^{f/-}$ MEFs were immortalized with E1A retrovirus and were subsequently infected with

either a control adenovirus or with an adenovirus-expressing Cre (gift from M. Cotten, GPC Biotech, Munich, Germany). Single-cell clones were selected and scored for p14 protein by Western blotting. For experiments involving starvation and mitogenic stimulation, MEFs were grown on fibronectin-coated dishes (10 μg/ml fibronectin). MEFs were growth arrested by contact inhibition and 48-h serum starvation. MEFs were released from the growth arrest by subconfluent replating in FCS-containing medium. KSR1$^{-/-}$ and KSR1$^{+/+}$ MEFs were provided by A.S. Shaw (Washington University School of Medicine, St. Louis, MO; Nguyen et al., 2002). MEK1$^{-/-}$ and MEK1$^{+/+}$ MEFs were gifts from M. Baccarini (University of Vienna and Medical University of Vienna, Vienna, Austria; Giroux et al., 1999; Galabova-Kovacs et al., 2006).

Epidermal barrier assay

Embryos were incubated for 8 h at 37°C in staining solution (1.3 mM $MgCl_2$, 100 mM $NaPO_4$, 3 mM $K_3Fe(CN)_6$, 3 mM $K_4Fe(CN)_6$, and 1 mg/ml X-Gal, pH 4.5, with HCl) according to Hardman et al. (1998).

Generation of retrovirus and infection

Mouse p14 and the p14caax cDNAs were subcloned into the retroviral transfer vector MMP (Klein et al., 2000). For retroviral gene transfer, embryonic fibroblasts were transduced at an MOI of 5 in the presence of 8 μg/ml polybrene (Sigma-Aldrich).

Statistics

The epidermis of at least four different mice for the respective phenotype was analyzed by counting positive cells per random field of view (at least 25). The mean was calculated with a SD in a confidence interval of $P < 0.001$. Growth curves of MEFs were evaluated in three independent experiments.

Endosome distance analysis

Images of LAMP1 immunofluorescence were acquired using a CCD camera (AxioCam HRC; Carl Zeiss MicroImaging, Inc.) on an epifluorescence microscope (Axiovert; Carl Zeiss MicroImaging, Inc.) at 16-bit data depth. Image analysis was performed with MATLAB software (The MathWorks) using custom-designed scripts. Nuclei were identified using the DAPI nuclear counterstain. The position of the geometric center of the nucleus was calculated for each cell and used as a parameter representative of the cell center. Individual endosomes were identified on the basis of their fluorescence intensities using a local thresholding approach. Endosome distances were binned in units of 2 μm in the range of 0 to 40 μm (from the nuclear center). The number of endosomes in each bin was used for further analysis. 24 *p14*$^{f/-}$ (1,804 late endosomes), 20 *Mek1*$^{+/+}$ (3,351 late endosomes), and 19 *p14*$^{-/-}$ cell (1,795 late endosomes) and 21 *Mek1*$^{-/-}$ (3,783) MEFs were analyzed. Results are given in relative frequencies (percentages) for each distance. Extreme cells (Fig. S2 B) were excluded from evaluation. A chi-square independence test was performed on the original data (sum of all endosomes per bin). Endosome distance distributions were found to be significantly different ($P < 0.001$).

Acquisition and processing of images

An imaging microscope (Axioplan2; Carl Zeiss MicroImaging, Inc.) with a 100× NA 1.3 oil objective (AxioPlan NeoFluar; Carl Zeiss MicroImaging, Inc.) was used for all images shown in Fig. 2 A and Fig. S2 B. For the acquisition of images, a camera (AxioCam HRc; Carl Zeiss MicroImaging, Inc.) and AxioVs40V4.5.0.0 software (Carl Zeiss MicroImaging, Inc.) were used. All fluorochromes (AlexaFluor568 donkey anti–goat IgG [H+L], AlexaFluor568 goat anti–mouse IgG [H+L], and AlexaFluor594 goat anti–rat IgG [H+L]) used in these two figures were purchased from Invitrogen.

A confocal laser-scanning microscope (LSM510 Meta; Carl Zeiss MicroImaging, Inc.) with a 63× plan-Apochromat NA 1.4 oil objective (phosphohistone 3; Carl Zeiss MicroImaging, Inc.) was used for all images shown in Figs. 1 C, 2 (C and D), 3 (C–E), 4 (A and B), and in Figs. S1 (G and H) and S2 A. For the acquisition of images, LSM Image Examiner software (version 3.1.0.117; Carl Zeiss MicroImaging, Inc.) was used. All fluorochromes (AlexaFluor488-dextran [mol wt of 10,000 kD; anionic fixable], AlexaFluor594-transferrin, AlexaFluor488-streptavidin complexed to EGF and biotinylated streptavidin, AlexaFluor488 goat anti–rabbit IgG [H+L], AlexaFluor568 goat anti–mouse IgG [H+L], AlexaFluor594 goat anti–rat IgG [H+L], AlexaFluor568 donkey anti–goat IgG [H+L], AlexaFluor568 donkey anti–goat IgG [H+L], and AlexaFluor568 donkey anti–goat IgG [H+L]) used in these figures were purchased from Invitrogen.

All immunofluorescence was performed at room temperature. In addition to the Zeiss software, images have been converted to Photoshop (version 9.0; Adobe). Brightness, contrast, or tonal value was improved, and figures were arranged with Macromedia Freehand MX 11.0 software (Adobe) and exported as jpeg files.

Primer sequences

The following primers were used: 152 (TGCGGTTTATTAGTAGTTGTGGTC), 153 (GTGCTACTGCATCGATCCTCTGTA), 154 (TACAGAGGATCGATGGCAGTAGCAC), 181 (GAAACGGTTGTGTAGTTCAGT), 180 (GTGCAATTCTGGAGCAGCTTC), 193 (AGCCTCTTGCTCTCCCTCAGT), 188 (GGGCACTGGGCAGCCCTGCCA), 194 (GCGACTGTAGGGGTGTGTTGG), 184 (GGCTTCTCCAGTGCTGTGTCT), 185 (AGACCTGCACCTGGCTCCTCT), 215 (GGTGACTACAACTCCCAGGCG), 202 (CAAGGGCATGCATAGATG), 218 (GAGTGGTTTCCTCGGGAGGAT), 208 (AATGGCCTCAACTCTCAGCTT), 170 (AGCTGGTTGCCGAACAGGATG), 219 (TGCACATGCATCCTGCCTGCT), and 220 (CTCATGGCAGGCAGGTGACTA).

Online supplemental material

The supplemental material contains a description and characterization of the conditional p14 allele, marker analysis of the p14-deficient epidermis, and a characterization of fluid phase endocytosis and recycling of transferrin in p14- and MEK1-deficient MEFs. Fig. S1 shows the targeting strategy, PCR genotyping, and Southern and Western blotting as well as differentiation and apoptosis markers in the epidermis. Fig. S2 shows that p14 is not required for transferrin receptor recycling and fluid phase endocytosis but is required for late endosomal positioning and EGFR degradation. Online supplemental material is available at http://www.jcb.org/cgi/content/full/jcb.200607025/DC1.

We are indebted to Erwin F. Wagner, Uta Möhle-Steinlein, Hans-Christian Theussel, and Rainer Zenz for help with embryonic stem cell work, blastocyst injection, and providing the MORE and K5-Cre2 transgenic mice and to Meinrad Busslinger and Abdallah Souabni for providing the Fple mice. We are grateful to Guenther Boeck for help with FACS analysis. We would like to thank Manuela Baccarini for providing Mek1$^{+/+}$ and Mek1$^{-/-}$ MEFs. We are also grateful to Kristian Pfaller and Angelika Floerl for the scanning electron microscope, Karin Gutleben for semithin sectioning, and Nikolaus Wick for mouse breedings.

Work in the Huber laboratory is supported by the special research program Cell Proliferation and Cell Death in Tumors (grant SFB021 from the Austrian Science Fund).

Submitted: 6 July 2006
Accepted: 20 November 2006

References

Acharya, U., A. Mallabiabarrena, J.K. Acharya, and V. Malhotra. 1998. Signaling via mitogen-activated protein kinase kinase (MEK1) is required for Golgi fragmentation during mitosis. *Cell*. 92:183–192.

Galabova-Kovacs, G., A. Kolbus, D. Matzen, K. Meissl, D. Piazzolla, C. Rubiolo, K. Steinitz, and M. Baccarini. 2006. ERK and beyond: insights from B-Raf and Raf-1 conditional knockouts. *Cell Cycle*. 5:1514–1518.

Giroux, S., M. Tremblay, D. Bernard, J.F. Cardin-Girard, S. Aubry, L. Larouche, S. Rousseau, J. Huot, J. Landry, L. Jeannotte, and J. Charron. 1999. Embryonic death of Mek1-deficient mice reveals a role for this kinase in angiogenesis in the labyrinthine region of the placenta. *Curr. Biol.* 9:369–372.

Hardman, M.J., P. Sisi, D.N. Banbury, and C. Byrne. 1998. Patterned acquisition of skin barrier function during development. *Development*. 125:1541–1552.

Jiang, C.K., T. Magnaldo, M. Ohtsuki, I.M. Freedberg, F. Bernerd, and M. Blumenberg. 1993. Epidermal growth factor and transforming growth factor alpha specifically induce the activation- and hyperproliferation-associated keratins 6 and 16. *Proc. Natl. Acad. Sci. USA*. 90:6786–6790.

Klein, C., H. Bueler, and R.C. Mulligan. 2000. Comparative analysis of genetically modified dendritic cells and tumor cells as therapeutic cancer vaccines. *J. Exp. Med.* 191:1699–1708.

Kolch, W. 2000. Meaningful relationships: the regulation of the Ras/Raf/MEK/ERK pathway by protein interactions. *Biochem. J.* 351:289–305.

Kornfeld, K., D.B. Hom, and H.R. Horvitz. 1995. The ksr-1 gene encodes a novel protein kinase involved in Ras-mediated signaling in *C. elegans*. *Cell*. 83:903–913.

Kurzbauer, R., D. Teis, M.E. de Araujo, S. Maurer-Stroh, F. Eisenhaber, G.P. Bourenkov, H.D. Bartunik, M. Hekman, U.R. Rapp, L.A. Huber, and T. Clausen. 2004. Crystal structure of the p14/MP1 scaffolding complex:

how a twin couple attaches mitogen-activated protein kinase signaling to late endosomes. *Proc. Natl. Acad. Sci. USA*. 101:10984–10989.

Morrison, D.K., and R.J. Davis. 2003. Regulation of MAP kinase signaling modules by scaffold proteins in mammals. *Annu. Rev. Cell Dev. Biol.* 19:91–118.

Muller, J., S. Ory, T. Copeland, H. Piwnica-Worms, and D.K. Morrison. 2001. C-TAK1 regulates Ras signaling by phosphorylating the MAPK scaffold, KSR1. *Mol. Cell*. 8:983–993.

Nguyen, A., W.R. Burack, J.L. Stock, R. Kortum, O.V. Chaika, M. Afkarian, W.J. Muller, K.M. Murphy, D.K. Morrison, R.E. Lewis, et al. 2002. Kinase suppressor of Ras (KSR) is a scaffold which facilitates mitogen-activated protein kinase activation in vivo. *Mol. Cell. Biol.* 22:3035–3045.

Pelkmans, L., E. Fava, H. Grabner, M. Hannus, B. Habermann, E. Krausz, and M. Zerial. 2005. Genome-wide analysis of human kinases in clathrin- and caveolae/raft-mediated endocytosis. *Nature*. 436:78–86.

Pullikuth, A., E. McKinnon, H.J. Schaeffer, and A.D. Catling. 2005. The MEK1 scaffolding protein MP1 regulates cell spreading by integrating PAK1 and Rho signals. *Mol. Cell. Biol.* 25:5119–5133.

Schaeffer, H.J., A.D. Catling, S.T. Eblen, L.S. Collier, A. Krauss, and M.J. Weber. 1998. MP1: a MEK binding partner that enhances enzymatic activation of the MAP kinase cascade. *Science*. 281:1668–1671.

Sibilia, M., and E.F. Wagner. 1995. Strain-dependent epithelial defects in mice lacking the EGF receptor. *Science*. 269:234–238.

Tallquist, M.D., and P. Soriano. 2000. Epiblast-restricted Cre expression in MORE mice: a tool to distinguish embryonic vs. extra-embryonic gene function. *Genesis*. 26:113–115.

Tarutani, M., S. Itami, M. Okabe, M. Ikawa, T. Tezuka, K. Yoshikawa, T. Kinoshita, and J. Takeda. 1997. Tissue-specific knockout of the mouse Pig-a gene reveals important roles for GPI-anchored proteins in skin development. *Proc. Natl. Acad. Sci. USA*. 94:7400–7405.

Teis, D., and L.A. Huber. 2003. The odd couple: signal transduction and endocytosis. *Cell. Mol. Life Sci.* 60:2020–2033.

Teis, D., W. Wunderlich, and L.A. Huber. 2002. Localization of the MP1-MAPK scaffold complex to endosomes is mediated by p14 and required for signal transduction. *Dev. Cell*. 3:803–814.

Therrien, M., H.C. Chang, N.M. Solomon, F.D. Karim, D.A. Wassarman, and G.M. Rubin. 1995. KSR, a novel protein kinase required for RAS signal transduction. *Cell*. 83:879–888.

Vasioukhin, V., C. Bauer, L. Degenstein, B. Wise, and E. Fuchs. 2001. Hyperproliferation and defects in epithelial polarity upon conditional ablation of alpha-catenin in skin. *Cell*. 104:605–617.

Wunderlich, W., I. Fialka, D. Teis, A. Alpi, A. Pfeifer, R.G. Parton, F. Lottspeich, and L.A. Huber. 2001. A novel 14-kilodalton protein interacts with the mitogen-activated protein kinase scaffold mp1 on a late endosomal/lysosomal compartment. *J. Cell Biol.* 152:765–776.